Underwater Hyperspectral Imaging, a new tool for Marine Archaeology

Øyvind Ødegård[1,2,*], Aksel Alstad Mogstad[3], Geir Johnsen[3], Asgeir J. Sørensen[1], Martin Ludvigsen[1]

[1] *Centre for Autonomous Marine Operations and Systems (NTNU AMOS), Department of Marine Technology, Norwegian University of Science and Technology (NTNU), Trondheim, Norway*
[2] *Department of Archaeology and Cultural History, University Museum, Norwegian University of Science and Technology (NTNU), Trondheim, Norway*
[3] *Centre for Autonomous Marine Operations and Systems (NTNU AMOS), Department of Biology, Norwegian University of Science and Technology (NTNU), Trondheim, Norway*
**Corresponding author: oyvind.odegard@ntnu.no*

Received XX Month XXXX; revised XX Month, XXXX; accepted XX Month XXXX; posted XX Month XXXX (Doc. ID XXXXX); published XX Month XXXX

By applying an Underwater Hyperspectral Imager (UHI) to a selection of archaeological artefacts, we have found spectral signatures that are representative of materials likely to be present at wreck sites. By successfully using the signatures to classify a subset of said artefacts placed on the seabed at 61 m depth, we demonstrate that it is possible to detect archaeological objects of interest (OOI) in UHI-data acquired by a remotely operated vehicle (ROV). Correct UHI-classification of rust and glass bottles *in situ* on a historical wreck site further supports the viability of the method for marine archaeological applications.

OCIS codes: *(110.4234) Multispectral and hyperspectral imaging; (010.4450) Oceanic optics.*

http://dx.doi.org/10.1364/AO.99.09

1. INTRODUCTION

Underwater Cultural Heritage (UCH) is defined as " [...] all traces of human existence having a cultural, historical or archaeological character which have been partially or totally under water, periodically or continuously, for at least 100 years[...]" [1]. One of the main categories of UCH is shipwrecks, which can be found in almost any body of trafficable water, and at all depths. Management of and research on underwater wreck sites are dependent on technologies to provide data. In shallow water diving technologies can bring archaeologists to the site directly, or remote sensing technologies can give indirect access. For deeper sites, the latter is currently the only practical way to gain knowledge.

Depending on how a ship wrecks, and the subsequent wreck site formation processes, a wreck deposited on the seabed could be in any state, from the structurally intact to the completely disintegrated with no organic materials preserved [2, 3]. In any case the composition of material remains will be complex to record, but at the same time very important for understanding and interpretation of the site.

The development in underwater robotics over the last decades have provided marine archaeology, and other fields in the marine sciences, with means to access deep or otherwise remote waters. Remotely Operated Vehicles (ROV) and Autonomous Underwater Vehicles (AUV) can be fitted with a range of sensors, and used to map large areas of seabed, or perform detailed close range investigations of interesting features on the seabed. Furthermore, advances in navigation and positioning control technologies embedded in such robots have enabled deployment of sensors that require precise and accurate maneuvering for data acquisition and processing.

Hyperspectral imagery is defined as images that contain a spectrum of reflected light with a spectral resolution of 1-5 nm per image pixel. Compositions of materials or objects of interest (OOI) will absorb, scatter and reflect light of different portions of the visible spectrum, giving them their own optical fingerprints that are unique, and can be used for classification with a high degree of confidence [4]. Using spectral libraries to classify materials in hyperspectral data is a well-established method, e.g. in geology [5]. In the last decade or so we have seen an increased use of hyperspectral imaging in remote sensing, and there are also examples of applications in archaeology [6-8]. Aerial sensor platforms like satellites and airplanes are currently common, but also smaller vehicles like drones have been used [9]. While some of these can do measurements in marine environments [10, 11], airborne methods are all passive (depend on ambient light), and are hence limited to shallow waters (<20m) [12]. By developing an instrument for deployment on underwater platforms, a range of new applications can be adopted [13]. Operating in environments with limited or no ambient light, lamps attached to the platform must be aligned with the field of view of the UHI to record reflected light from OOI. In

addition to the OOI, the inherent optical properties of the water will affect the spectrum of the reflected light [14].

Underwater hyperspectral imaging is a novel technology, and currently there are only a few studies published on applications and results from field experiments [13-17]. UHI technology has been used to record selected areas on two archaeological wreck sites, the Reference wreck in Trondheim harbor [18] and the Figaro in Trygghamna in Svalbard [19].

The intention of this paper is to explore the suitability of UHI as a tool for UCH investigation, and propose a method for UHI-based classification in marine archeology. The main scientific contribution is the development of a spectral library of signatures from a selection of materials likely present on many UCH sites. We will compare their characteristics using Principal Component Analysis (PCA), and then use selected spectral signatures for supervised spectral angle mapper (SAM) classification of a subset of these objects imaged in an uncontrolled environment. Finally we will do a supervised classification of UHI images acquired at a wreck site with relevant objects or materials identified by HD video. We will propose that UHI imaging will be a valuable new method for detection and investigation of UCH. To the authors' knowledge this study is the first application of UHI technology to investigate UCH, and should be regarded as an initial study on the field.

In section 2A we present a selection of materials for laboratory measurements and subsequent deployment on a frame on the seabed. Section 2B describes the UHI and how it was set up with different platforms in the laboratory and at field trials. Section 2C describes reflectance conversion, PCA and SAM classification. The results from spectral analyses and classifications are presented in section 3. In section 4 we discuss results, and the suitability of the method for marine archaeological applications. Concluding remarks are made in section 5.

2. METHODS and MATERIALS

A. Materials

From the definition of UCH above it follows that materials that can typically be present at UCH sites encompass everything from fossilized tree trunks in submerged paleo landscapes, to the inventory of RMS Titanic. To limit the range of relevant materials to fit the scope of an initial study of a new method, the materials selected for this study (Fig.1) have been collected from seabed surface findings at marine archaeological surveys in Mid Norway, and generally assumed to be from the 18th and 19th century. The selection can be considered to be typical for objects occurring at Nordic or Northern European modern era wreck sites – but is not purported to be comprehensive for any site inventory. Also the selection was to some degree limited to materials that could be expected to still be present and exposed on the seabed after a 3-400 years long wreck site formation process (i.e. mainly inorganic materials).

The OOI have been organized in three main categories, ceramics, metals and glass. In addition, a few other objects were measured and put in a group called "other".

Fig.1. Selection of archaeological artefacts made of materials likely to be present at modern era Northern European wreck sites.

1. *Ceramics*

Ceramics is a collective term used for basically any heat-treated clay, and can typically be encountered at wreck sites in variations from fine China porcelain and clay pipes to roof tiles and crude bricks. Fractures and untreated surfaces are typically dull, from deep red-brown to off-white or creamy in color, depending on clay type and manufacturing process. For a thorough overview of the material characteristics of ceramics in general, the reader is referred to Henderson [20]. Surface treatment for decorative or practical purposes is typically glazing, which produces a very glossy possibly colored surface. Decorations could be done by adding different colored components to a lead glazing, e.g. uranium oxide for red, cobalt for blue, copper oxide for green [21]. Pottery is ubiquitous at archaeological sites, also underwater. Pots and pans used as containers, for cooking or eating were consumer commodities with a short life span. Bricks were commonly used in constructing galleys or other fireplaces on board ships for hundreds of years. Clay pipes were made for hundreds of years by different producers in different countries.

In this paper, three different types of bricks, a variety of pottery shards, glazed and unglazed, and a selection of clay pipe stems were used to acquire spectral signatures of ceramics. Age and provenance were not determined.

2. *Metals*

Different types of metals are commonly found on wreck sites. Anchors, chains, tools, guns, bolts and nails were all commonly iron-based artefacts aboard modern European ships. Iron exposed to seawater corrodes relatively fast, often leaving just formless lumps of red oxide, commonly known as rust. In this paper, we used a corroded iron ball of unknown date and function to acquire a spectral signature for rust.

Brass is a copper alloy not uncommonly found on modern era wreck sites, e.g. lanterns or bolts. It corrodes lightly, and attains a decorative green surface without decomposing. We measured a lightly corroded brass weight of unknown date and function to acquire a spectral signature.

In addition a lead weight, a spoon (assumed silver), a pocket watch and a coin were scanned in the laboratory. All

were of unknown age and provenance. The spoon and the coin were characterized by distinct patches of corrosion.

3. *Glass*

Glass, especially bottles, is a very typical and common find category on modern era European wreck sites. The chromatic characteristics can vary from colorless to colored and from transparent to opaque determined by the presence and combinations of several different dissolved, amorphous or crystalline materials and production processes [20]. Utility glass bottles were often made of so-called black glass, a term used for dark brown or dark green glass [22]. In this paper we measured seven bottles (or fragments thereof) in laboratory, and five of those were also put on the underwater frame. None of the bottles were dated, but most likely none were older than AD 1800. The bottles were selected to represent a variety in color and translucence.

4. *Other*

Until the advent of steel ships in late 19th century wood has been the dominant building material for larger ships and boats all over the world. A single piece of wood planking was scanned, species and age was not determined. In addition a piece of coal, a piece of animal bone and two pieces of dark flint (partially with cortex) were scanned. They are all materials likely to be found on a wreck site.

B. Sensor and platforms

All measurements presented in this paper were acquired using a 4th generation push-broom UHI produced and developed by Ecotone AS (Trondheim, Norway). A scan line (1X1920 pixels) was imaged synoptically with the camera slit oriented perpendicular to the along track direction. Opening angle was 60 ° across track and 0.4 ° along track. The UHI measured in the wavelength range 370-800 nm with 0.9 nm spectral resolution. The UHI camera had a 12 bit radiometric resolution. The hyperspectral unit was coupled with a 5 MP video camera providing time stamped video frames of the UHI field of view for all measurements. All data were stored locally on the UHI sensor on an integrated SSD unit. Data was acquired and recorded using Immersion software (Ecotone AS).

The UHI has a 355 x 135 mm titanium housing. It is depth rated to 3000 m, and can be used by different robotic platforms (see discussion).

1. *Laboratory set-up*

In the laboratory at Trondheim Biological Station, NTNU (Trondheim, Norway) the selection of archaeological OOI was submerged in a plastic tank filled with sand filtered sea water (from 100 m depth). The UHI was mounted on a motorized rig on top of the tank to move with controlled speed along a horizontal track perpendicular to the sensor slit (Fig.2). The sensor was placed at a fixed altitude of 43 cm above the bottom for all measurements, moving at an along track speed of 0.06 ms^{-1} during scanning. Across track spatial resolution was approximately 0.2 mm.

There was no artificial light in the room (lights off), only some limited ambient daylight through the blinded windows (all measurements were done before noon on one single day in July 2017) to avoid other light sources than the UHI lamps. This was done to avoid any further light corrections of data from the UHI scanning tank. Two diffused 250 watt halogen lamps with known spectral signatures were spaced 20 cm at either side of the UHI sensor which was vertically aligned and

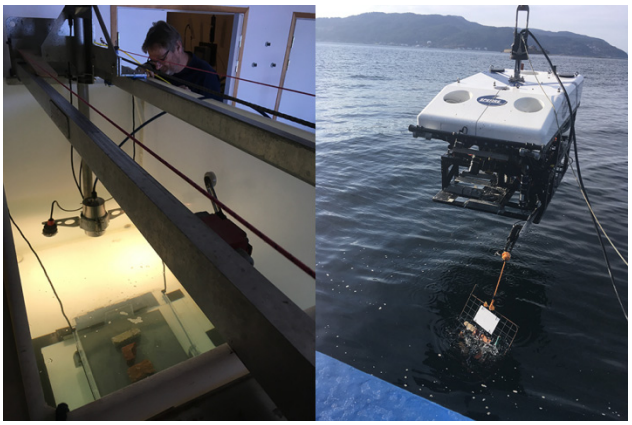

Fig.2 To the left: tank with UHI mounted on motorized rig for scanning of objects of interest (OOI). To the right: Subfighter 30 K ROV with OOI frame ready to be deposited on the seabed near the wreck site.

angled to provide an even illumination of the UHI's field of view.

A calibrated Spectralon reflectance standard plate (Labsphere Inc., USA) reflecting 99% of visible light in the 400-700 nm range was used for "white light" and lamp reference, together with a white polyethylene (PE, sanded to avoid specular reflection) plate. The reference plates were placed next to the OOIs, and were included in all measurements to be used as a corrective to derive reflectance values. Camera focus was manually adjusted before measuring. The UHI was set with a 2.8 aperture (to ensure optimal focus depth range and light transmitted to sensor), and recorded at 20 frames per second with a 30 millisecond exposure time for each frame.

2. *Field set-up*

The "Reference Wreck" in Trondheimsfjorden (63°27'12,466"N 10°24'23,66"E), is a late 17th century wooden wreck situated at 61 m depth in the extension of the outlet from the river Nidelva, outside Trondheim harbor. The wreck site has served as a testing ground for research on robotic platforms and sensors by the Applied Underwater Robotics Laboratory at NTNU [18, 23]. The wreck site covers an area of about 30 m x 20 m, and the seabed in the area is characterized by sand and gravel. The most prominent feature on the site is a keelson with some frames that barely protrudes from the sediments. Frequent visits with the ROV to the site in the period 2012-2017 have shown that sediments are shifting, probably caused by river currents, occasionally exposing and covering parts of the wreck's structural elements as well as moving objects on the site, e.g. bottles and loose pieces of planking.

A selection of the OOI measured in lab were mounted to a steel frame (1m x 1m) together with a white sanded PE reference plate identical to the one used in the lab (Fig.3). The steel frame was placed on the seabed in close proximity to the wreck (< 10 m).

The robotic platform was a work class Subfighter 30 K ROV (Fig. 2) from Sperre AS (Notodden, Norway) with dynamic positioning (DP) capabilities, enabling it to perform

very accurate navigation such as station keeping and path following [24].

UHI data quality, as typical for push broom sensors, is

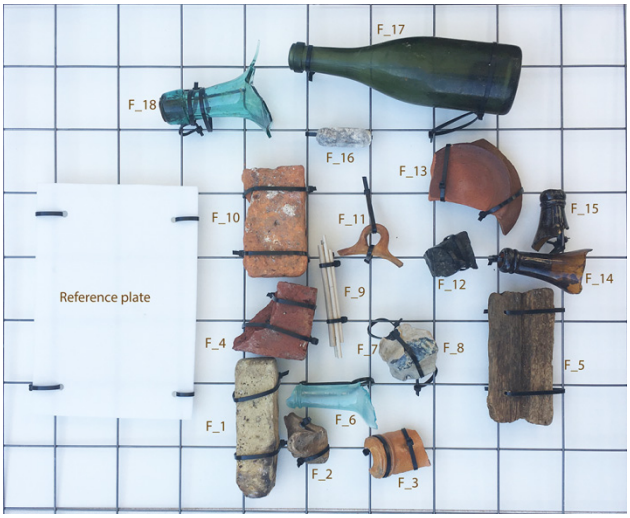

Fig.3 A selection of objects scanned in the laboratory were attached to a metal frame with a reference plate, and deposited on the seabed next to the reference wreck site in Trondheimsfjorden, Norway.

sensitive to changes in speed, altitude, pitch, roll and yaw[14]. This makes ROVs with DP capabilities very well suited as platforms. Additionally, it makes it possible to tap into the navigational data logs, and thus provide time stamped sensor data with spatial references for geo-referencing purposes. The 30 K ROV was deployed from the DP capable research vessel RV Gunnerus. The UHI was mounted looking downward at the lower center of the ROV, with two 250 W halogen lamps (identical to the ones used in the laboratory measurements, but without diffusers) for illumination. The UHI was set with a 2.8 aperture and recorded at 25 frames per second with a 40 millisecond exposure time for each frame. Spectral binning was set to 2, i.e. recording bands at approximately 0.9 nm. Spatial binning was set to 2 due to low light.

A short UHI transect was made over the known OOI frame, and thereafter three 30 m x 1 m UHI transects with 3 m line spacing were made over the wreck site. All UHI transects, both of the frame and the wreck site, were done at 1.5 m altitude and at 0.2 ms^{-1} speed. Across track spatial resolution was approximately 0.9 mm. Except for the two halogen lamps, all lights on the ROV were turned off during the UHI recording.

C. Data processing and analyses

Due to noise in the outer bands all analyses were applied to spectral subsets limited to visible light between 470-690 nm wavelengths, excluding the extreme ends of the spectrum (low signal to noise ratio caused by the lamps used).

The raw image files from the laboratory were resized spatially in ENVI using 1st degree rotation, scaling and translation (RST) algorithm (with nearest neighbor resampling) factoring 6.46 in the along-track direction. The resulting images (viewed as RGB) were used to select regions of interest (ROI) for spectral analysis. ROI size could vary from 1 to 25 pixels, depending on the object size. The UHI-transects of the OOI frame and wreck were resized the same way as the laboratory images, but with a factor of 8 in the along-track direction. The UHI-transects from the wreck site were subsequently georeferenced for GIS layering in ArcGIS using a first order polynomial transformation. All ROIs, endmember extraction and classifications were done in the original size flat field corrected image files. Resized versions were only used for visualization and guidance.

1. *Raw data to reflectance conversion*

Raw-data consists of the digital counts the UHI sensor makes at the different wavelengths. It can be seen as the sum of upwelling radiance reflected from the OOI, reflections from scatterers in the water column and ambient light. In addition there is noise inherent in the sensor. Reflectance is a percentage of how much light at each wavelength is reflected off the OOI, independent of illumination and the optical properties of the water column. Reflectance at a given wavelength can be expressed as

$$R(\lambda) = \frac{L_u(\lambda)}{E_d(\lambda)} \quad \textbf{(1)}$$

where $L_u(\lambda)$ is the upwelling radiance, and $E_d(\lambda)$ is downwelling irradiance. For Eq. 1 to hold true, all surfaces are assumed to behave like Lambertian reflectors.

In the laboratory measurements, every scan was done with a sanded white PE plate placed in the tank next to the OOI. In ENVI, the Flat Field Correction algorithm was used to divide all pixels in every scanned image on the average spectral signature of the white reference plate. We assume ideal lightning such that measured radiance of an object is independent of its position on the scan line. Additionally, the reference plate is assumed to reflect the downwelling radiance equally at all wavelengths. Given these assumptions, the calculation of true reflectance for any OOI is

$$R_t(\lambda) = \frac{L_{u\,ooi}(\lambda)}{L_{u\,ref}(\lambda)} \quad \textbf{(2)}$$

where $L_{u\,ooi}(\lambda)$ and $L_{u\,ref}(\lambda)$ are the spectral upwelling radiance from the OOI and reference plate respectively.

The same procedure was used for the OOI frame data set (from the seabed), using the attached reference plate. During deployment of the frame some sediment particles were whirled up and settled on the plate. We can assume that as a consequence less light was reflected from the plate, and thus producing images with on average exaggerated intensity values per pixel from the flat field correction conversion. Possible skewing effects this could have across the spectrum were difficult to estimate, and were not considered in the following analyses.

2. *Principal Component Analysis*

To assess the spectral relationship between different objects and materials, principal component analyses (PCAs) were performed on the laboratory-acquired reflectance data. The principal components can be seen as the axes in an ellipsoid with n dimensions that describes the data. The longest axis accounts for the largest variance in the data, and corresponds to principal component 1 (PC1). The second longest axis corresponds to PC2, and so on. Using the open source statistical software R, the PCAs were performed on standardized data (mean = 0, variance = 1), at 1-nm spectral resolution. PCA results were illustrated in biplots generated using the ggbiplot package, available from GitHub (GitHub Inc., USA: https://github.com/vqv/ggbiplot). In the biplots, points representing individual measurements, ellipses

representing group-specific 95% confidence intervals, and arrows representing the different wavelength variables were used to interpret the results of the analyses. Points that are near each other in the plot are likely to have spectral similarities.

3. Classification

To build a spectral library (endmembers) the Spectral Library Builder tool in ENVI was used. For each OOI, ROIs were selected at perceived representative homogenous surfaces, avoiding shadows and highlights. At least three ROIs were selected for each object. ROI size varied from one to 25 pixels.

Continuing in ENVI, the Spectral Angle Mapper (SAM) tool was used to classify selected UHI images in the spectral range 470-690 nm. There are many algorithms available for spectral classification, SAM was chosen for its speed, simplicity and ease of use [25]. The SAM algorithm compares the angle between the endmember spectrum vector and each image pixel vector in n-D space [26]. The process produced rule images that could be analyzed using the Rule Image Classifier tool, finding the optimal maximum angle threshold for each class.

Since we were only able to confidently identify bottles, rust and wood in the wreck transects – classifications based on other signatures were not considered meaningful since results could not be verified by physical sampling and examination.

3. RESULTS

A. Laboratory – spectral analysis

In four consecutive scans, spectral properties of 31 objects were scanned (Fig.4). Signatures from ROIs were averaged and organized in a spreadsheet, and subjected to a principal component analysis.

Results from the PCAs are displayed in Fig. 5. The upper part (a) shows the biplot from the object-specific PCA, whereas the lower part (b) shows the biplot from the PCA performed on grouped categories. In the biplots, object/group-specific points clustered closely together indicate consistent optical signatures. Ellipses represent the 95% confidence intervals of the various objects and groups, and non-overlapping ellipses may be interpreted as objects/groups being spectrally distinguishable from each other. In both biplots, PC1 and PC2 respectfully explain 83.9 and 15.8% of the total spectral variance. Considering that this adds up to 99.7%, taking into account additional principal components (PCs) was regarded as unnecessary.

The PCA biplots for the objects measured in lab [Fig.5(a)] indicates that a grouping of some materials based on spectral characteristics could be carried out. The ceramics category shows that the unglazed/untreated pottery shards (L_4 through L_10 in fig.4) together with two of the bricks (L_1 and L_2) conjoined to a tight cluster of data points. The other objects in the category; the yellow brick (L_3), clay pipes (L_34-L_36), the selters (L_28) and genever (L_33) bottle fragments, were more widely distributed in the plot. Of the seven glass bottles, all except for two (L_17 and L_23) completely overlapped in the PCA biplot – apparently good candidates for a group. The metal category proved to be spectrally inconsistent, and thus not suitable for grouping. Even the measurements for the individual objects proved to be incoherent, indicating very heterogeneous or patched surfaces. The measurements of the rusted iron ball (L_16) were relatively aggregated in the plot, and overlapped almost completely with the ceramics group. Of the remaining objects in the 'other' category, wood (L_30) and bone (L_31) measurements were relatively close, indicating possible spectral semblance. Coal (L_32) ended up in the middle of the concentration of bottle measurements. The dark flint measurements formed a relatively united group of measurements, while the flint cortex measurements were widely scattered. Figure 5 (b) shows a PCA biplot of groups of materials and objects selected for use in classification.

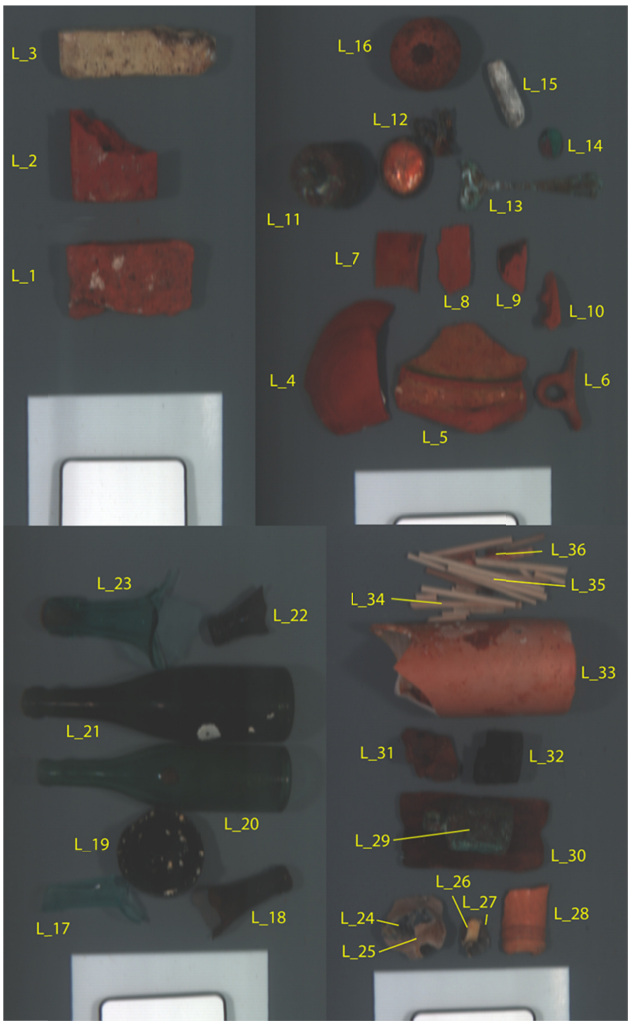

Fig.4. Four scans of 31 objects with reference plates done in laboratory. Annotations correspond to spreadsheet in appendix X. The images have been stretched by a factor of 6.46 in the Y-axis for better visual presentation. Three clay pipes were measured (L_34-L_36) to comprise differences in hue. Additional measurements were done of the flint pieces to include cortex (L_24-L_27). Brass weight was measured in two scans (L_11 and L_29)

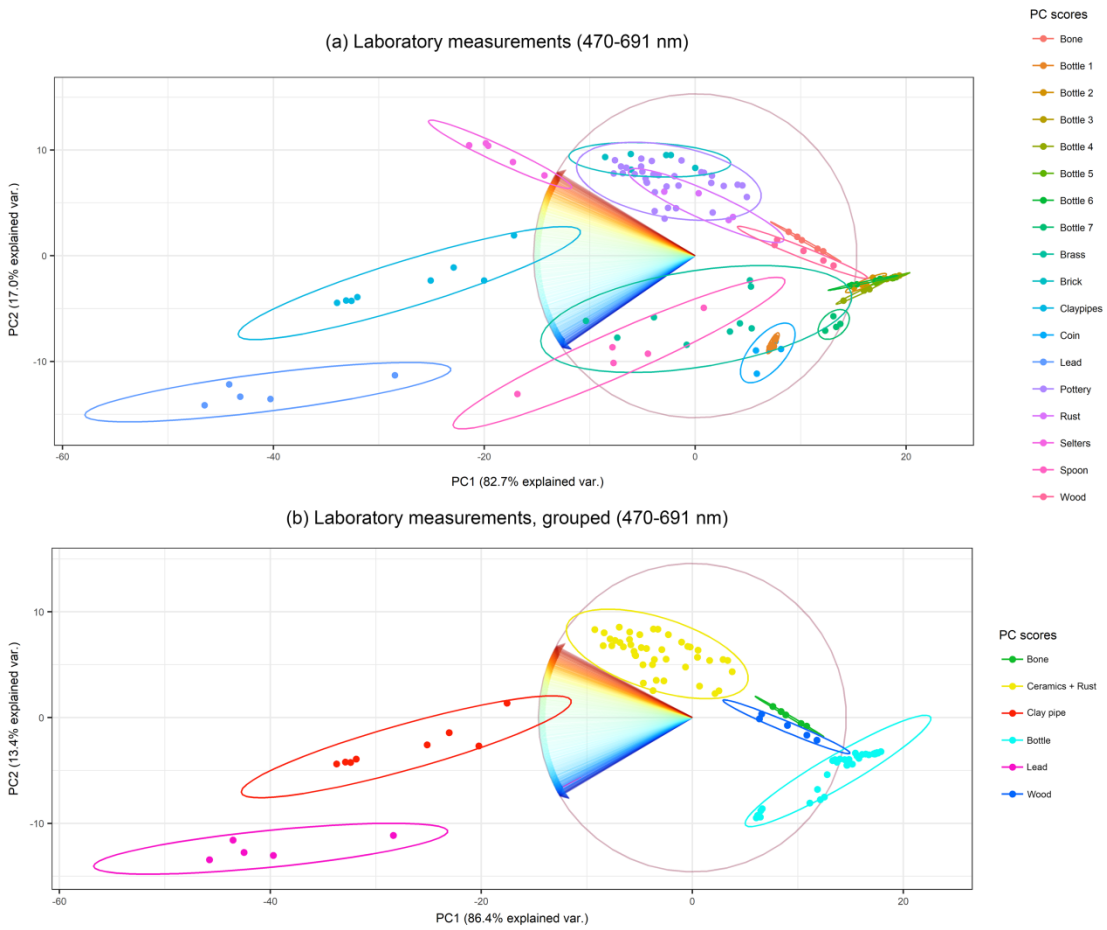

Fig. 5 Principal Component Analysis (PCA) plots of objects scanned by UHI in laboratory. The following objects formed too indistinct plot distributions and were excluded from the PCA analysis: the yellow brick (L_3), the genever (L_33) bottle fragment, both pieces of flint (L_24-L_27), the spoon (L_13), the piece of coal (L_32) and the watch (L_12). The lower PCA plot (b) shows the groups and objects selected for classification

B. Classification

1. *Frame*

Figure 6(a) shows signatures for bone, wood, clay pipes, ceramics, bottle and lead from the spectral library that were used to perform a SAM classification of the object frame. In Fig. 6(b) we can see signatures from the same objects measured on the frame *in situ*. In Fig. 7 the UHI-transect of the OOI frame is overlaid with color coded classification results, and an error matrix with classification accuracy is presented in Table 1. Bone was only partly classified (17%), but on the other hand there was almost no misclassification. Wood was only partly classified (30%), and also misclassified over 50% of the bone object. Clay pipes were classified relatively accurately (34%) but misclassified all of a light yellow brick and parts of the flint cortex. Ceramics was accurately classified (71%), including the glazed selters bottle fragment. Two of the bottles were accurately classified, but three were almost completely missed. Lead was relatively accurately classified (37%), but misclassified parts of the clay pipes. Coal, flint and flint cortex failed to do any meaningful classification, and in addition produced considerable misclassifications.

2. *Wreck*

Data from the three transects of the wreck site were converted to reflectance by a flat field correction based on the PE reference plate on the OOI frame. In one transect we could confirm presence of several materials by studying HD video: conglomeration of rust, two bottles (probably of later date, and suspected to not be part of the original wreck inventory) and some exposed wood. A subset containing all these materials was selected for classification (Fig.8).

Rust was classified using both ceramic and rust signatures from the spectral library. As can be seen in Fig.9 both had instances of misclassification. The ceramic signature classified the identified rust features more completely than the rust signature, but also had more instances of misclassification. The two bottles were successfully classified, with modest misclassification. The wood classification failed, with very modest correct classification, and substantial misclassification.

Table 1 Error matrix for classification of OOI frame

	Clay pipes	Bone	Wood	Lead	Ceramics	Bottle	Total
Unclassified	50	27.05	69.55	62.76	9.93	77.63	47.84
Clay pipes	34.13	0	0	0	18.79	0	8.17
Bone	0	17.21	0.27	0	0	0	0.39
Wood	0	51.64	30.18	0	0.17	0.2	4.95
Lead	15.87	0	0	37.24	0	0	1.25
Ceramics	0	4.1	0	0	71.1	0	28.22
Bottle	0	0	0	0	0	22.17	9.18
Total	100	100	100	100	100	100	100

Table 1. Error matrix with ground truth in columns and classification in rows. All numbers are given in percent.

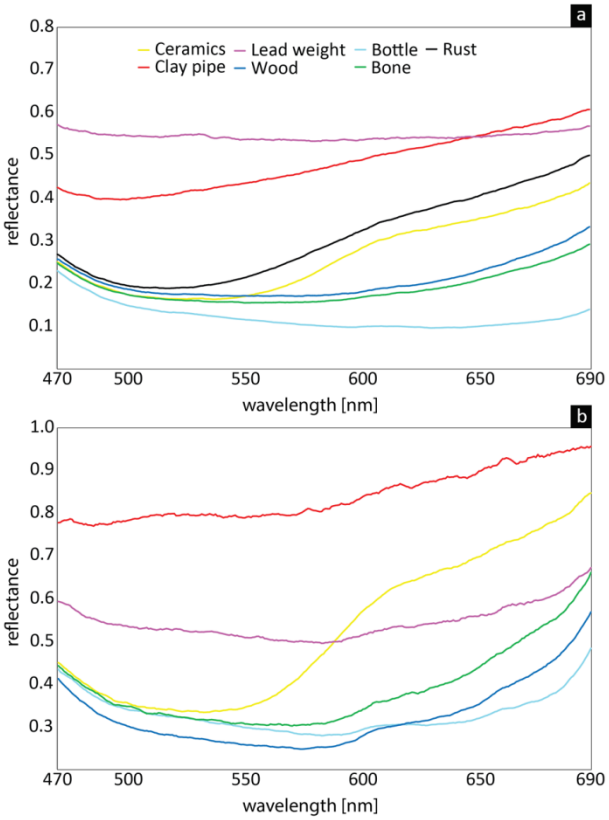

Fig. 6. a) Signatures from the spectral library acquired in laboratory used as training set for classification of OOI on frame and the reference wreck transect. b) Spectral signatures of OOI on frame measured *in situ*.

4. DISCUSSION

The results presented in this paper indicate that spectral characteristics are suitable for classification of archaeological OOI likely to be present at wreck sites. The PCA biplots indicate that most of the sampled fragments of ceramics and bottles can be grouped based on similar spectral characteristics. It is also clear that the spectral signature of the rusted iron object is indistinguishable from most of the ceramics. The selected metals apparently do not share spectral characteristics that would justify a group.

The SAM classification of the OOI frame supports the PCA biplots, demonstrating that several ceramics and bottles can be classified with a common signature. Considering how both group classifications omitted some objects completely (three bottle fragments and one of the bricks), it is possible that more than one group signature per material category could be appropriate.

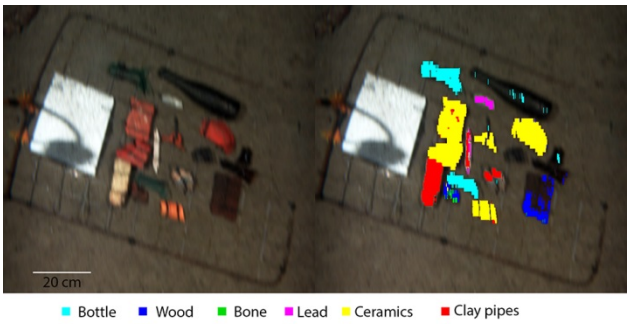

Fig. 7 UHI images of metal frame with OOI deposited on the seabed adjacent to the reference wreck. Image to the right shows SAM classifications based on spectral library created in laboratory (misclassifications of the white reference plate and nylon rope have been removed).

Furthermore, the classification of OOIs on the frame demonstrates consistency in data quality when changing platform and environment from laboratory to field experiment. Noise in the outer bands of the visible spectrum seems to be similar in laboratory and in situ data, and limiting analyses and classification to signatures in the 470-690 nm range was deemed appropriate for all data (future experiments with other lamp types should be conducted to possibly expand the applicable spectral range). The shapes of the OOI's spectral signatures measured in laboratory and *in situ* are relatively similar (fig.6), and thus suitable for classification with the SAM algorithm that only considers vector angle, not length [26]. Overall the results from supervised classifications of the OOI frame were relatively accurate. Classification of the wreck transect confirms the method's ability to classify, and hence detect, rust and bottles *in situ* using spectral signatures acquired from laboratory measurements. The very overlapping results from classifications with ceramics and rust signatures, supports the grouping of the two materials in the PCA biplot (fig. 5). As can be seen in fig. 6 (a), the shapes of the spectral signatures of rust and ceramics follow each other closely. Features with optical fingerprints resembling those of archaeological materials occur naturally in the oceans. Organisms containing e.g. astaxanthin-protein pigments may be spectrally similar to rust/ceramics and indeed, a few squat lobsters (*Galathea* sp.) were erroneously classified as rust/ceramics in the wreck transect. Given that the abundance of different seafloor organisms (measured in biomass) decreases as a function of depth [22], misclassification of natural features as probable wreck materials could be expected to abate in deeper waters. Taking this into consideration, statistical and spatial reasoning about density and abundance of classes should perhaps be integrated in the detection algorithms thus reducing the amount of false positives. Strategies for automated assessments of detection confidence have been developed for onshore hyperspectral imaging [27], and a similar approach could be relevant for UHI detection as well.

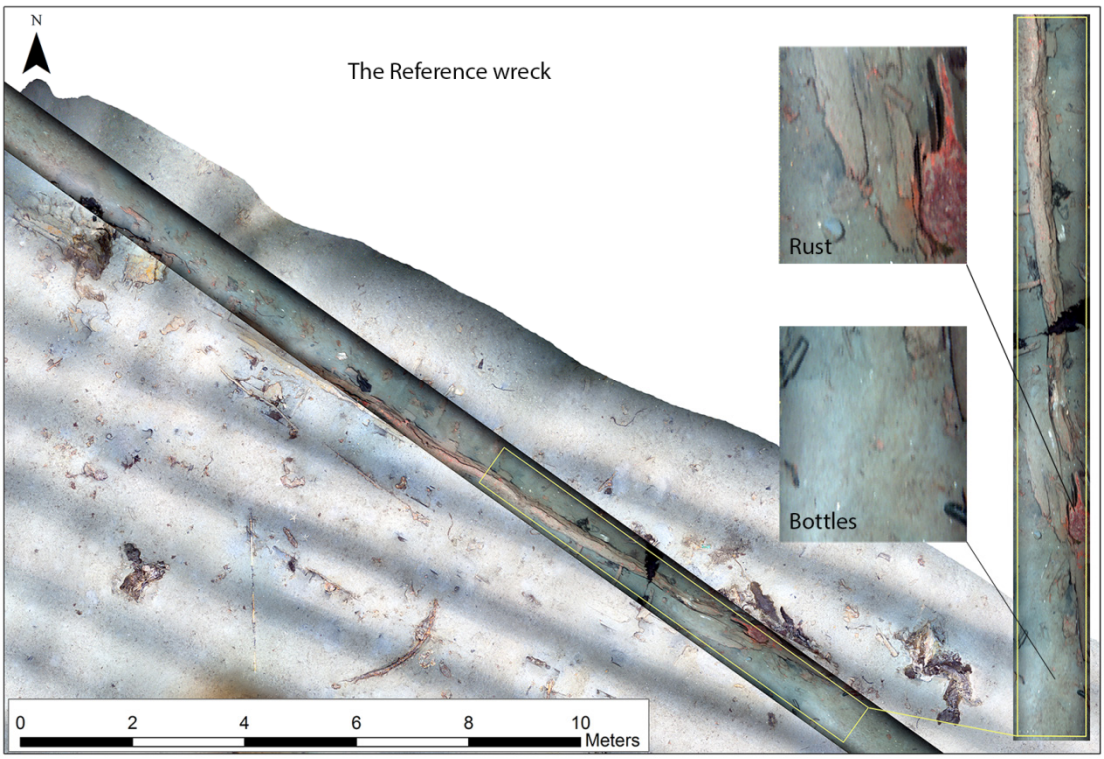

Fig. 8 The Reference wreck. Photomosaic from stereo camera with UHI transect overlay showing area (yellow frame) selected for classification.

Sedimentation is a site formation process affecting all cultural heritage deposited on the seabed, and at a rate determined mainly by local environmental factors. Additionally, biological organisms (epi-growth or microbial bio film) can be expected to cover exposed surfaces over time. It is not known how this will affect UHI imaging as described in this paper. The OOI frame was left on the seabed, and frequent revisits to establish time series for answering these questions are planned.

Using UHI to detect underwater cultural heritage sites could potentially be a method of great benefit for seabed mapping. UHI has already been successfully deployed on an AUV in deep waters [28]. With spectral libraries on board, AUVs on long duration mapping surveys could autonomously verify possible wreck sites registered by other longer range sensors, e.g. as described in [29]. During such surveys it is not likely that reference material (PE plates or equivalent) would be available, and other methods for achieving reflectance conversion dealing with the IOPs in the water column would have to be applied.

Many of the objects measured to provide spectral characteristics for typical wreck site materials have not been precisely identified with regards to provenance and date. Production and material composition of these objects would have varied with time and place of production, and possibly also from depositional environment over hundreds of years. The reason for this is that signatures diagnostic for different material groups have been the goal, not the exact spectral signature for the specific artefacts. This could undoubtedly be of great value for many mapping applications, but would be of limited use for an initial study as presented in this paper. A more exact identification and pure spectral analysis of OOI similar to the design of other libraries [30, 31] will very likely be relevant for future applications. The inclusion of the Spectralon reflectance standard plate in the laboratory scans ensures that we can convert to true reflectance values for the objects presented in this paper, suitable for such a libraries.

Future work should expand the selection of reference materials to ensure better spectral representation of OOI. We believe experiments with different samples of waterlogged wood could be of particular relevance for detection of wreck sites and for enhancement of classification success.

5. CONCLUSION

In this paper we have presented the first application of UHI on ROV to identify and map archaeological OOI at an UCH site. We have demonstrated the ability to use images of selected materials in a controlled light environment to create spectral signatures for groups of materials likely to be present at many wreck sites. These signatures have been used to successfully classify objects of interest *in situ* at a wreck site. This indicates that UHI detection and classification of OOI represents a promising new method for marine archaeological seabed mapping.

Acknowledgment

This work has been carried out at the Centre for Autonomous Marine Operations and Systems (AMOS). The Norwegian Research Council is acknowledged as the main sponsor of AMOS through the Centres of Excellence funding scheme, Project number 223254. The authors wish to thank the crews of RV Gunnerus and AUR-Lab for much help with data acquisition.

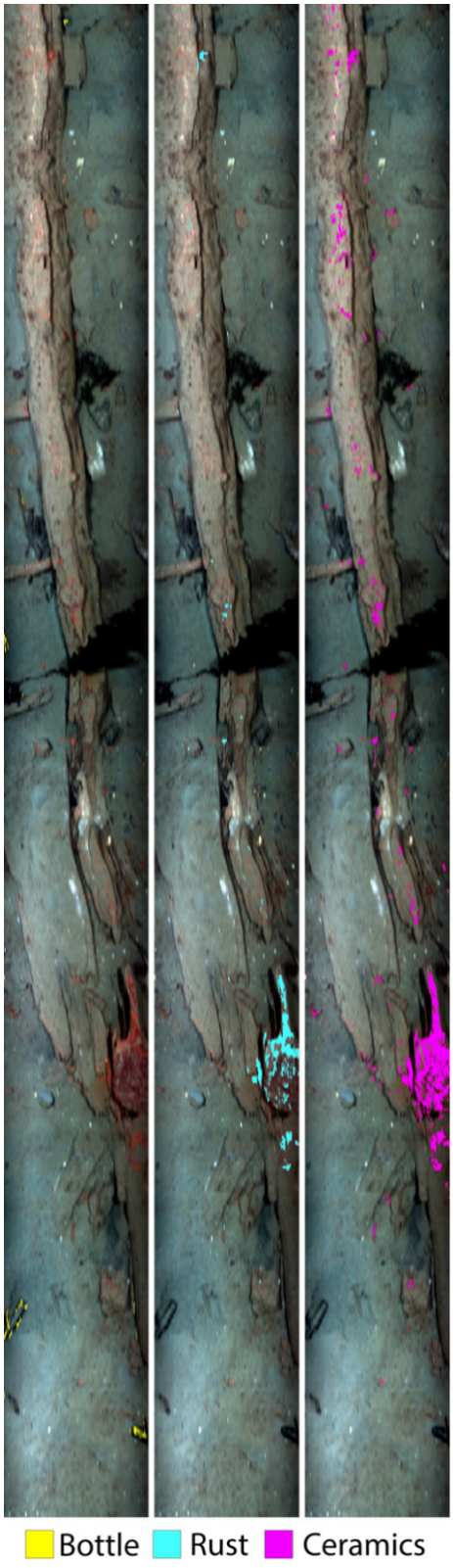

Fig. 9 Supervised SAM classifications of UHI-based photomosaic of wreck transect. From left: glass bottle, rust and ceramics. The transect measures 0.75 m x 8 m.

References

1. UNESCO, "The UNESCO Convention on the Protection of the Underwater Cultural Heritage," U. G. C. C, ed. (2001).
2. K. Muckelroy, *Maritime archaeology* (Cambridge University Press, 1978).
3. D. J. Stewart, *Formation Processes Affecting Submerged Archaeological Sites: An Overview* (1999), Vol. 14, pp. 565-587.
4. C. D. Mobley, L. K. Sundman, C. O. Davis, J. H. Bowles, T. V. Downes, R. A. Leathers, M. J. Montes, W. P. Bissett, D. D. Kohler, and R. P. Reid, "Interpretation of hyperspectral remote-sensing imagery by spectrum matching and look-up tables," Applied Optics **44**, 3576-3592 (2005).
5. F. D. van der Meer, H. M. A. van der Werff, F. J. A. van Ruitenbeek, C. A. Hecker, W. H. Bakker, M. F. Noomen, M. van der Meijde, E. J. M. Carranza, J. B. d. Smeth, and T. Woldai, "Multi- and hyperspectral geologic remote sensing: A review," International Journal of Applied Earth Observation and Geoinformation **14**, 112-128 (2012).
6. M. Doneus, G. Verhoeven, C. Atzberger, M. Wess, and M. Ruš, "New ways to extract archaeological information from hyperspectral pixels," Journal of Archaeological Science **52**, 84-96 (2014).
7. S. H. Savage, T. E. Levy, and I. W. Jones, "Prospects and problems in the use of hyperspectral imagery for archaeological remote sensing: a case study from the Faynan copper mining district, Jordan," Journal of Archaeological Science **39**, 407-420 (2012).
8. M. J. Abrams and D. C. Comer, "Multispectral and Hyperspectral Technology and Archaeological Applications," in *Mapping Archaeological Landscapes from Space* (Springer, 2013), pp. 57-71.
9. A. Lucieer, Z. Malenovský, T. Veness, and L. Wallace, "HyperUAS—Imaging Spectroscopy from a Multirotor Unmanned Aircraft System," Journal of Field Robotics (2014).
10. Z. Volent, G. Johnsen, and F. Sigernes, "Kelp forest mapping by use of airborne hyperspectral imager," Journal of Applied Remote Sensing **1**, 011503-011503-011521 (2007).
11. H. M. Dierssen, "Overview of hyperspectral remote sensing for mapping marine benthic habitats from airborne and underwater sensors," in 2013), 88700L-88700L-88707.
12. P. R. C. Fearns, W. Klonowski, R. C. Babcock, P. England, and J. Phillips, "Shallow water substrate mapping using hyperspectral remote sensing," Continental Shelf Research **31**, 1249-1259 (2011).
13. G. Johnsen, M. Ludvigsen, A. Sørensen, and L. M. S. Aas, "The use of underwater hyperspectral imaging deployed on remotely operated vehicles-methods and applications," IFAC-PapersOnLine **49**, 476-481 (2016).
14. G. Johnsen, Z. Volent, H. Dierssen, R. Pettersen, M. Van Ardelan, F.Søreide, P. Fearns, M. Ludvigsen, M. Moline, "Underwater hyperspectral imagery to create biogeochemical maps of seafloor properties," in *Subsea optics and imaging* (Woodshead Publishing Limited, 2013).
15. R. Pettersen, G. Johnsen, P. Bruheim, and T. Andreassen, "Development of hyperspectral imaging as a bio-optical taxonomic tool for pigmented marine organisms," Organisms Diversity & Evolution **14**, 237-246 (2014).
16. I. Dumke, S. M. Nornes, and M. Ludvigsen, "First hyperspectral survey of the deep seafloor: DISCOL area, Peru Basin," in *EGU General Assembly Conference Abstracts*, 2017), 4529.
17. A. A. Mogstad and G. Johnsen, "Spectral characteristics of coralline algae: a multi-instrumental approach, with emphasis on underwater hyperspectral imaging," Applied Optics (In press).

18. Ø. Ødegård, A. J. Sørensen, R. E. Hansen, and M. Ludvigsen, "A new method for underwater archaeological surveying using sensors and unmanned platforms," IFAC-PapersOnLine **49**, 486-493 (2016).
19. M. Daase, "Cruise Report - Polar Night Cruise 2016," (Tromsø, 2016).
20. J. Henderson, *The science and archaeology of materials: an investigation of inorganic materials* (Routledge, 2013).
21. I. W. Reed, *Trønderkeramikk: "adskillige sorter krustøi"* (Tapir akademisk forl., Trondheim, 2009), p. 239 s. ill.
22. W. Van Den Bossche, "Antique Glass Bottles: Their History and Their Evolution (1500-1850)," Antique Collector's Club, Wappinger's Falls, New York (2001).
23. F. Søreide, "Cost-effective deep water archaeology: preliminary investigations in Trondheim Harbour," International Journal of Nautical Archaeology **29**, 284-293 (2000).
24. A. J. Sørensen, F. Dukan, M. Ludvigsen, D. A. Fernandes, and M. Candeloro, "Development of dynamic positioning tracking system for the ROV Minerva," in *Further Advances in Unmanned Marine Vehicles,* G. Roberts and B. Sutton, eds. (2012), pp. 113-128.
25. S. Shanmugam and P. SrinivasaPerumal, "Spectral matching approaches in hyperspectral image processing," International Journal of Remote Sensing **35**, 8217-8251 (2014).
26. F. Kruse, A. Lefkoff, J. Boardman, K. Heidebrecht, A. Shapiro, P. Barloon, and A. Goetz, "The spectral image processing system (SIPS)—interactive visualization and analysis of imaging spectrometer data," Remote sensing of environment **44**, 145-163 (1993).
27. M. A. Kolodner, "Automated target detection system for hyperspectral imaging sensors," Applied optics **47**, F61-F70 (2008).
28. Ø. Sture, M. Ludvigsen, and L. M. S. Aas, "Autonomous underwater vehicles as a platform for underwater hyperspectral imaging," in *OCEANS 2017-Aberdeen*, (IEEE, 2017), 1-8.
29. Ø. Ødegård, S. M. Nornes, M. Ludvigsen, T. J. Maarleveld, and A. J. Sørensen, "Autonomy in Marine Archaeology," in *CAA2015 Keep the Revolution Going: Proceedings of the 43rd Annual Conference on Computer Applications and Quantitative Methods in Archaeology*, (Archaeopress, 2016), 857-865.
30. R. N. Clark, G. A. Swayze, R. Wise, K. E. Livo, T. M. Hoefen, R. F. Kokaly, S. J. Sutley, and M. Team, "USGS Digital Spectral Library splib05a," US Geological Survey, Open File Report **3**, 395 (2007).
31. A. Baldridge, S. Hook, C. Grove, and G. Rivera, "The ASTER spectral library version 2.0," Remote Sensing of Environment **113**, 711-715 (2009).